The 9th European Congress on Computational Methods in Applied Sciences and Engineering
ECCOMAS Congress 2024
3–7 June 2024, Lisboa, Portugal

A SYNTHETIC BUBBLE MODEL AS INLET FOR FLUID-STRUCTURE INTERACTION SIMULATIONS WITH TWO-PHASE FLOW

Henri Dolfen[1] **and Joris Degroote**[1,2]

[1] Department of Electromechanical, Systems and Metal Engineering, Ghent University, Sint-Pietersnieuwstraat 41, 9000, Ghent, Belgium, henri.dolfen@ugent.be

[2] Flanders Make, Ghent, Belgium

Key words: Computational fluid dynamics, Two-phase flow, Fluid-structure interaction, Flow-induced vibrations, Tube bundle

Summary. One of the challenging aspects about interface-resolved numerical simulation of two-phase flows is the correct representation of the conditions at inlet boundaries, which can lead to inaccuracies if they are not realistic [1].

For a flow regime with large gas bubbles, a long precursor domain can be used in which these bubbles develop, but this incurs a substantial computational cost. Therefore a different approach is used here, namely the Synthetic Bubble Model (SBM), developed by De Moerloose et al. [2]. This model creates a transient, non-uniform inlet profile which produces gas bubbles from the inlet, instead of relying on the break-up of a steady, continuous gas jet. The result is a reduced mesh size upstream of the region of interest. The technique has been tested by De Moerloose et al. [2] for the forces acting on rigid tube bundles, yielding satisfactory results. The current research takes it one step further, and also investigates the resulting vibration.

To this end, fluid-structure interaction simulations of a tube bundle experiment in a cross-flow air/water-mixture are performed with the SBM at the inlet. In the experimental setup, air is injected in a water channel, after which the mixture enters the test section. The flow is conditioned by a few rows of rigid rods, with one or multiple moving rods located downstream. They are considered rigid bodies and their motion is enabled by mounting them on a flexible blade. Given that flow-induced vibrations are dominated by liquid impact, the Volume of Fluid approach is opted for. The vibrations are analyzed and the SBM technique for accurate representation of the inlet is validated by comparing the forces with the experimental values.

1 INTRODUCTION

Many two-phase flows exhibit complicated, transient and erratic flow patterns which pose challenges to their numerical simulation. Lumping the intricate and ever changing interface into the subgrid scales results in closure models that require adequate calibration. If instead the interface is resolved, like in the Volume of Fluid (VOF) method, other difficulties arise.

This paper focuses on the representation of this interface at the inlet boundary in interface-resolved, Eulerian methods such as VOF. One option observed in literature is the supply of steady (gas) jets [1, 2] or stratified flow [3] at the inlet, neglecting transient behavior. Another option is to start with an unresolved interface by setting an average void fraction at the inlet [4],

relying on the model to develop a sharp interface further downstream. Both options require a long development length upstream of the zone of interest [3], entailing additional computational cost, or if this upstream domain is too short, the solution may be affected [1].

Two-phase flows occur in many shell-and-tube type heat exchangers such as condensers, evaporators and steam generators. The fluctuating forces caused by the two-phase cross-flow can cause damage to steam generators if too severe [5]. Unscheduled outages of pressurized water nuclear reactors are in 25 % of the cases related to problems in the steam generator [6].

Understanding flow-induced vibrations (FIV) in steam generators better is one of the goals of the GO-VIKING project [7], which this research is part of. For a review of previous experimental and numerical work, the reader is referred to the paper of Benguigui et al. (2024) [5]. Two-phase flow patterns are of primary interest in characterizing FIV and the obtained regime depends on the geometry as well as on how the two-phase flow is generated and introduced [5, 8]. Benguigui et al. [5] identify the need for deeper understanding of the inlet parameters.

Fluid-structure interaction (FSI) simulations, coupling a two-phase computational fluid dynamics (CFD) solver to a structural model, only took off recently as a research approach for FIV with multiphase flow, examples being the thesis of Benguigui (2018) [9] and the paper of Sadek, Mohany and Hassan (2018) [10]. Assuming that FIV excitation is dominated by large gas structures, the VOF approach is a good choice. Its limited use so far for this type of investigations can partly be related to the difficulty in providing correct inlet conditions. De Moerloose et al. [3] contributed to the research by offering a novel inlet modeling approach: the Synthetic Bubble Model (SBM), implemented in Python[1]. In the absence of detailed inlet data, the SBM creates a reasonable, transient inlet condition, avoiding long precursor domains (see Section 3.1).

The first contribution of the current work is making the SBM compatible with Ansys Fluent, besides OpenFOAM. The modified SBM is tested on a larger bundle than has been used in the original validation [3], namely the TITAN experiment [11], a smaller scale abstraction of a steam generator. Moreover, it is the first use of the SBM with a two-way coupled FSI simulation.

The rest of the paper is structured as follows. In Section 2 the experiment is briefly introduced, after which the numerical methods are discussed in Section 3. Finally, in Section 4, the CFD-only results are discussed first, comparing different VOF implementations, followed by the FSI results.

2 EXPERIMENT

The TITAN experimental setup [11] shown in Figure 1 is hosted by CEA (Commissariat à l'énergie atomique et aux énergies alternatives) in Paris, France. The test section contains a rotated triangular tube array subject to an upward air/water flow. Due to an upstream air/water mixer, the air bubbles are assumed to be homogeneously distributed.

The tubes have a diameter D of 30 mm and a length L of 300 mm, which is also the channel depth. The channel width is 224.5 mm. The shortest distance between two tube centers, called the pitch P is equal to 43.2 mm, resulting in a pitch-to-diameter ratio P/D of 1.44.

Up to 15 tubes can be made flexible by mounting them on a flexible blade, as is shown in Figure 1b. As the blade is much stiffer in one direction than in the perpendicular direction, it is essentially a 1-dimensional vibration. The first mode natural frequency f_n is 22.5 Hz and the damping ratio ζ is 0.35 % [11]. In this case, a single flexible tube is considered, vibrating in the

[1] `https://github.com/pyfsi/SBM`

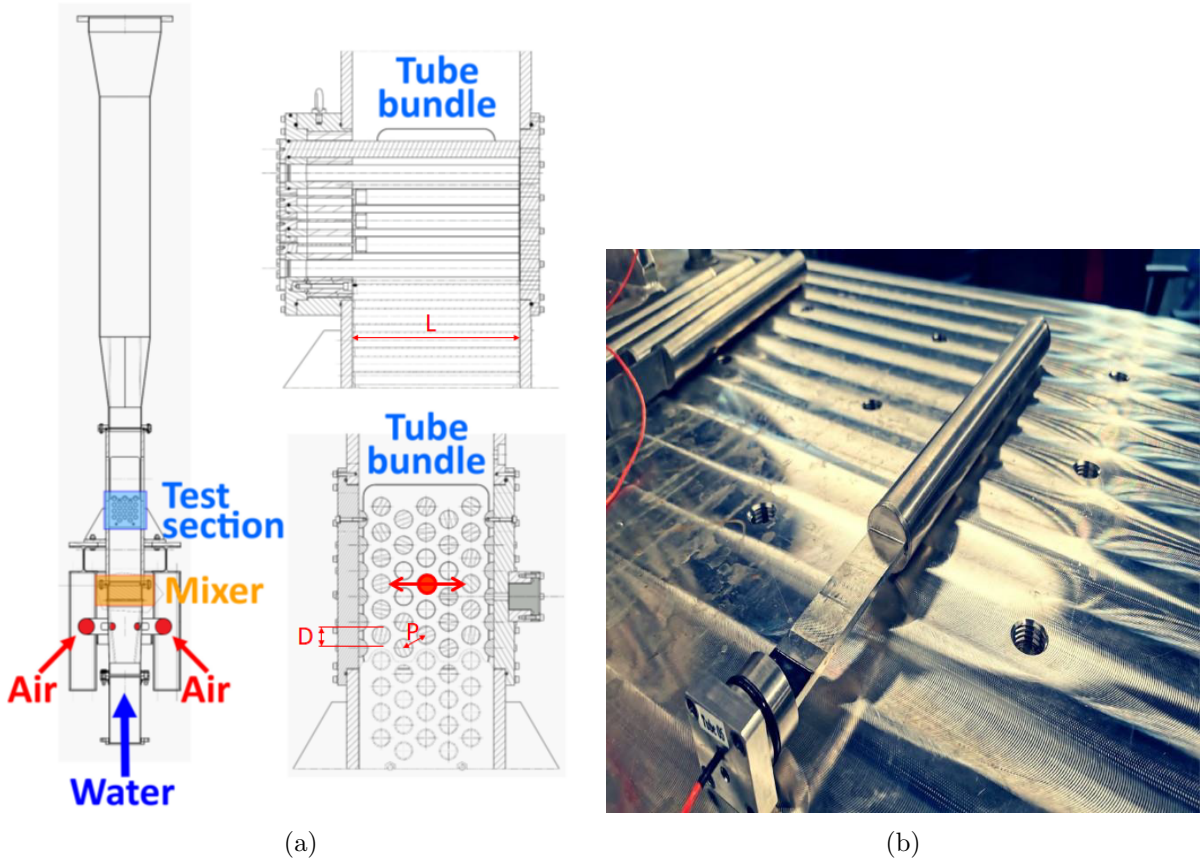

(a) (b)

Figure 1: The experimental setup [11]. (a) Schematic of the experimental loop, with indication of the tube that is used for either force measurements or vibration measurements. (b) Picture of the tube with flexible mount.

horizontal direction as shown in Figure 1a. As will be explained in Section 3.3, it was modeled as a 1 degree-of-freedom oscillator.

3 NUMERICAL METHODOLOGY

3.1 The Synthetic Bubble Model

The main idea of the SBM is to create a virtual (i.e. without flow calculation) pre-domain which extends the faces of the inlet plane perpendicularly with a user-defined number of layers, equal to the foreseen number of time steps. The SBM sets the value of the volume fraction of the phases for each cell of the pre-domain. At each time-step a new layer of this pre-domain is fed to the inlet plane, serving as the inlet profile for the void fraction.

The flowchart in Figure 2 visually explains how the SBM prepares the virtual pre-domain. In the following explanation water and air will be used as example for the phases. The algorithm starts with creating a pre-domain with the number of layers equal to the number time steps set by the user and initializing it to pure water ($\alpha_{water} = 1$). A variable m_{def} keeps track of the mass of the gas that has been defined and is initially put on 0. Following parameters related to the

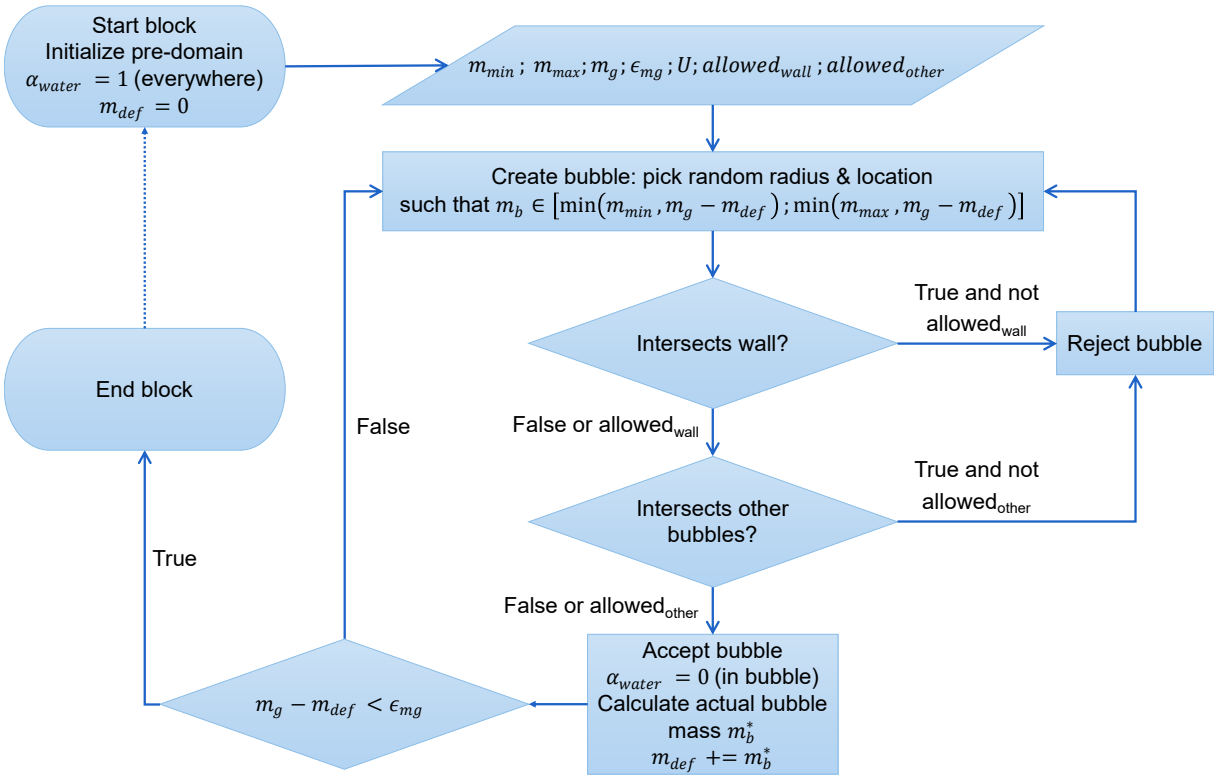

Figure 2: Simplified flowchart of the Synthetic Bubble Model. Not included are details on the initialization of the pre-domain, detection of intersections and the calculation of m_b^*.

bubbles are specified by the user: m_{min} and m_{max}, the mass of the smallest and largest possible bubble respectively, m_g, the total mass of gas that needs to be defined, U, the velocity at the inlet and $allowed_{wall}$ and $allowed_{other}$, two boolean parameters defining whether the bubbles are allowed to intersect the walls of the domain and each other respectively.

After initialization, a loop is started which adds gas to the domain. A bubble is created at a random location, the size (mass m_b) of which is in principle random, but constrained by m_{min} and m_{max}. Here, uniform distributions are used for the random samples, but other ones can also be used, if known from experiments for example. When the remaining amount of gas to be injected $m_g - m_{def}$ becomes less than first m_{max} and then m_{min}, it becomes the respective constraint instead. Next, it is checked whether the bubble intersects with the wall or previously defined bubbles. The bubble is then rejected or accepted according to the user's specifications. If it is accepted, the cells of the virtual pre-domain are updated to have $\alpha_{water} = 0$ and the actual mass of the bubble m_b^* is computed to update m_{def}. This loop is repeated until the difference between the defined mass m_{def} and the desired mass is below the tolerance ϵ_{mg}. In the course of this work, this loop was implemented more efficiently, realizing a speed-up of the generation of the virtual pre-domain by a factor of 20 compared to the original implementation.

This procedure can be repeated for a new pre-domain if more data is needed, as in [2], but it is recommended to generate all data required for the simulation at once, because otherwise the introduction of bubbles is briefly interrupted, introducing spurious periodicity and statistically non-uniform void fractions in time.

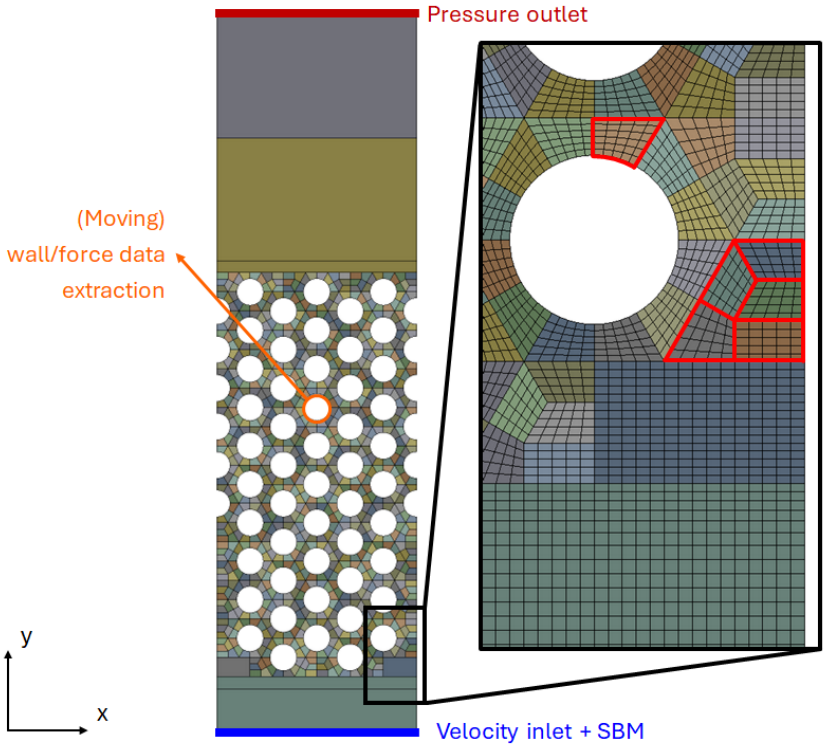

Figure 3: Flow domain and mesh.

Besides introducing bubbles in a random fashion, the SBM could easily be extended to include data, for instance from a wire mesh sensor, thanks to its ability to apply a time-dependent inlet profile in Fluent and OpenFOAM. It is worth noting that the SBM allows the user to specify the bubble size distribution in any case, but that this choice may affect the results [5, 8].

3.2 Flow model

A depiction of the block-structured flow mesh can be found in Figure 3. The unit blocks of which the tube bundle region consists (highlighted in red) have 5×5 or 5×6 divisions. The maximal aspect ratio in this region is 2.18 and only in the last block before the outlet (gray) the cells gradually become longer in the flow direction to an aspect ratio of 5 to smoothen the fields towards the outlet for numerical stability. The minimal orthogonal quality is 87 %. The inlet and outlet plane have 90×125 faces and the entire mesh totals 4 188 750 cells.

The flow is solved with Ansys Fluent 2023R1, using the unsteady Reynolds-averaged Navier–Stokes equations with the k-ω SST turbulence model. The velocity inlet was augmented with the SBM for the void fraction, providing homogeneously distributed bubbles. Inlet data was generated for 12 000 time steps of 0.0005 s. Both phases were introduced with a uniform velocity $U = 0.25\,\mathrm{m/s}$, thus neglecting slip. Buoyancy and surface tension forces are assumed to further develop the flow while traveling through the rigid bundle, before it reaches the zone of interest with the moving rod. Given the volume fraction of air $\alpha_{air} = 40\,\%$, this gives volume flow rates $Q_{water} = 10.1\,\mathrm{l/s}$ and $Q_{air} = 6.75\,\mathrm{l/s}$. This means that for a total simulated time of 6 s,

a mass of air m_g of 0.049 612 5 kg must be defined in the virtual pre-domain, up to a tolerance chosen as 1×10^{-5} kg. Settings m_{min} and m_{max} were taken 0.000 165 375 kg and 0.000 413 437 5 kg respectively, or 2 % and 5 % of the average amount of air introduced per second (0.008 268 75 kg). Both intersection between the bubbles and with the walls were allowed. The flow leaves the domain through a pressure outlet.

The experiment operates at room temperatures, so the density of air ρ_{air} was taken 1.225 kg/m^3 and its dynamic viscosity μ_{air} 1.7894×10^{-5} Pa s, while for water $\rho_{water} = 998.2\,\mathrm{kg/m^3}$ and $\mu_{water} = 1.003 \times 10^{-3}$ Pa s was used. A surface tension of 0.072 75 N/m was specified.

For the Volume of Fluid method both an implicit and explicit formulation exist [12]. For the latter, the cell value of the volume fraction of the current time step is directly calculated based on the known fluxes at the previous time step. Both methods were tested in this paper. This was combined with both 1$^{\text{st}}$ order and 2$^{\text{nd}}$ order (bounded) implicit time stepping for all other flow variables. Note that for explicit VOF, only 1$^{\text{st}}$ order time discretization is allowed in Fluent. In order to stabilize convergence in all time steps, a velocity limiter was employed.

The lift forces on the cylinder indicated in orange in Figure 3 were monitored when it was rigidly mounted. When it was flexibly mounted, these forces were communicated to a rigid body solver in a two-way FSI loop, as described in the next section.

3.3 Rigid body solver

The rigid body motion coupled with the flow is solved in an iterative FSI procedure, as demonstrated by Vierendeels et al. [13]. The procedure is outlined below.

The flexibly mounted cylinder is assumed to behave as a single degree-of-freedom mass-spring-damper system, of which the x-direction motion is described by

$$m\ddot{x} + c\dot{x} + kx = F, \tag{1}$$

m being the mass, c the damping, k the stiffness and F the force from the flow simulation. Writing this in an implicitly coupled FSI loop gives

$$m\ddot{x}^{n+1,k+1} + c\dot{x}^{n+1,k+1} + kx^{n+1,k+1} = F^{n+1,k+1}. \tag{2}$$

In this formulation, n represents the time step and k the coupling iteration. The derivative $\partial F/\partial\ddot{x}$ can be used to compute a better approximation of the force at cylinder's new position:

$$\begin{aligned} F^{n+1,k} + \frac{\partial F}{\partial \ddot{x}}\left(\ddot{x}^{n+1,k+1} - \ddot{x}^{n+1,k}\right) &= m\ddot{x}^{n+1,k+1} + c\dot{x}^{n+1,k+1} + kx^{n+1,k+1} \\ \Leftrightarrow \ddot{x}^{n+1,k+1}\left(\frac{\partial F}{\partial \ddot{x}} - m\right) &= -F^{n+1,k} + c\dot{x}^{n+1,k+1} + kx^{n+1,k+1} + \frac{\partial F}{\partial \ddot{x}}\ddot{x}^{n+1,k}. \end{aligned} \tag{3}$$

The following Newmark time integration scheme allows further substitutions:

$$\dot{x}^{n+1,k+1} = \dot{x}^n + (1-\beta)\Delta t\ddot{x}^n + \beta\Delta t\ddot{x}^{n+1,k+1} \tag{4}$$

$$x^{n+1,k+1} = x^n + \Delta t\dot{x}^n + \gamma\Delta t^2\ddot{x}^n + \alpha\Delta t^2\ddot{x}^{n+1,k+1}. \tag{5}$$

This finally results in

$$\ddot{x}^{n+1,k+1} = \frac{F^{n+1,k} - \frac{\partial F}{\partial \ddot{x}}\ddot{x}^{n+1,k} - c\left[\dot{x}^n + (1-\beta)\Delta t\ddot{x}^n\right] - k\left[x^n + \Delta t\dot{x}^n + \gamma\Delta t^2\ddot{x}^n\right]}{m + c\beta\Delta t + k\alpha\Delta t^2 - \frac{\partial F}{\partial \ddot{x}}}. \tag{6}$$

The force on the moving cylinder $F^{n+1,k}$ is calculated with the flow solver at every coupling iteration k, leading to a new prediction of the displacement through the acceleration $\ddot{x}^{n+1,k+1}$. This displacement is implemented in the flow simulation by deforming the mesh in the arbitrary Lagrangian–Eulerian (ALE) mesh motion framework. The iteration loop is repeated until the residual $\|m\ddot{x} + c\dot{x} + kx - F\|$ has decreased 3 orders of magnitude.

Eq. (6) requires knowledge of the derivative $\partial F/\partial \ddot{x}$, which is not generally available. Therefore it is estimated in the first coupling iteration of each time step using a perturbation δ on the acceleration:

$$\ddot{x}^{n+1,k=0} = \ddot{x}^{n}, \qquad \ddot{x}^{n+1,k=1} = \ddot{x}^{n} + \delta. \tag{7}$$

It can then be approximated by the finite difference

$$\frac{\partial F}{\partial \ddot{x}} \approx \frac{F^{n+1,k=1} - F^{n+1,k=0}}{\ddot{x}^{n+1,k=1} - \ddot{x}^{n+1,k=0}} = \frac{F^{n+1,k=1} - F^{n+1,k=0}}{\delta}, \tag{8}$$

where F results from the CFD simulation given a certain acceleration $\ddot{x}$. A value of $\delta = 0.1\,\mathrm{m/s^2}$ was found to work well for this simulation. For the Newmark scheme, $\alpha = 1.0$, $\beta = 1.0$ and $\gamma = 0.0$ were used, which is a backward Euler scheme.

As only the natural frequency and damping ratio were available from the experiment (see Section 2), the mass and stiffness values could not uniquely be determined. Based on a similar setup [14] the following values were assumed for the preliminary FSI simulations in this paper: $m = 1.34\,\mathrm{kg}$, $c = 1.326\,44\,\mathrm{N\,s\,m^{-1}}$ and $k = 26\,788.6\,\mathrm{N/m}$.

4 RESULTS

4.1 Flow patterns in rigid bundle

As mentioned in Section 3.2, different formulations of the VOF method were used. Two simulations were run with the implicit formulation, one employing a 2$^{\mathrm{nd}}$ order bounded implicit time scheme and one with a 1$^{\mathrm{st}}$ order implicit scheme. No convergence was achieved with an unbounded 2$^{\mathrm{nd}}$ order scheme. Finally, a simulation with the explicit VOF formulation was also run, 1$^{\mathrm{st}}$ order implicit in time for the other flow variables.

A snapshot of the void fraction after 5 s of flow time is shown in Figure 4. One can observe big similarities between Figure 4a and Figure 4b, the two simulations using the implicit VOF formulation. The gas structures seem more diffuse and elongated compared to the explicit VOF result shown in Figure 4c. The latter exhibits more compact bubbles with sharper interfaces.

Figure 5 compares the histogram of values of α_{air}, including each cell in the domain, except those in the outflow region with increasing aspect ratio, for the three cases. It can be seen that the explicit VOF histogram is strongly peaked to the extreme values, while for the implicit VOF formulation more intermediate values of α_{air} are found. This is in line with the observations in Figure 4, where the implicit method seems more diffuse. As the difference between 1$^{\mathrm{st}}$ order and 2$^{\mathrm{nd}}$ order time discretization is limited, it is unlikely that the time discretization error has a large contribution to this diffusivity.

Intermediate values of α_{air} would also occur when the bubble sizes become smaller than the grid resolution. Studies towards the bubble sizes and grid resolution, combined with the VOF formulation, have yet to be performed and are therefore not included in this paper. Since the same virtual pre-domain was used for the three different cases, the SBM has no contribution

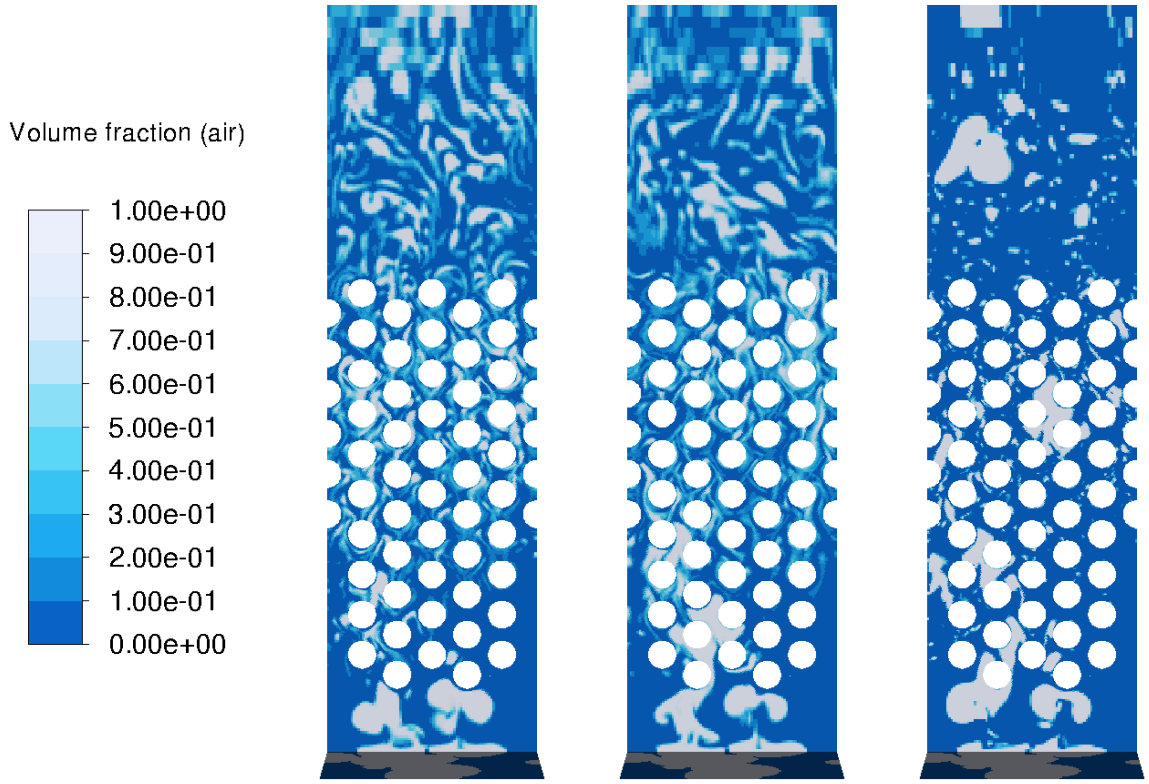

Figure 4: Color plot of the void fraction α_{air} after 5 s. (a) Result for the implicit VOF formulation, using a bounded 2$^{\text{nd}}$ order implicit time scheme. (b) Result for the implicit VOF formulation, using a 1$^{\text{st}}$ order implicit time scheme. (c) Result for the explicit VOF formulation, using a 1$^{\text{st}}$ order implicit time scheme for the other variables.

to these discrepancies. All three results confirm that the SBM manages well to introduce an interface-resolved (Eulerian) unsteady two-phase flow at the inlet, mimicking the random nature of the flow, as will also be evidenced by the forces scrutinized in the next section.

4.2 Forces on rigid cylinder

The lift force on the (stationary) cylinder (indicated in red in Figure 1) versus time is plotted in Figure 6 together with experimental data. The signals are seen to cover approximately the same range. The intermittent impact of the gas bubbles results in an erratic signal with many peaks. The signal from the explicit VOF simulation exhibits this behavior to the largest extent, although at a higher amplitude than in the experiment. The simulations using the implicit VOF formulation predict a smoother signal, because the bubbles are smeared out more, especially the 1$^{\text{st}}$ order simulation.

When plotting the results in the frequency domain (Figure 7), it is seen that all three simulations predict a broad peak in the low frequency band (0 Hz–20 Hz). As expected from Figure 6,

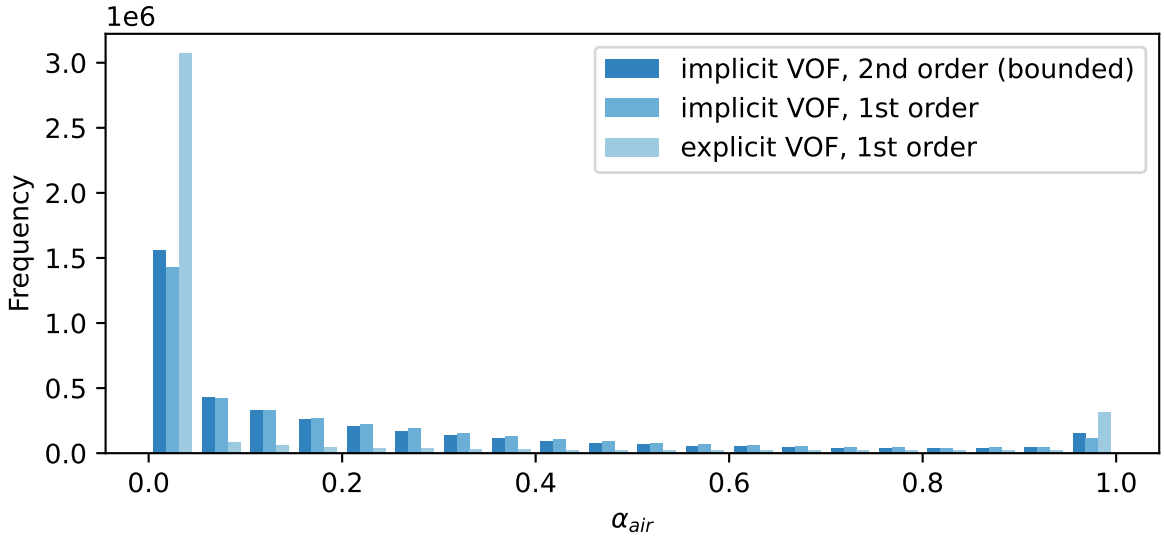

Figure 5: Histogram of the α_{air} cell values found in the domain after 5 s, excluding the outflow region with increasing aspect ratio (see Figure 3).

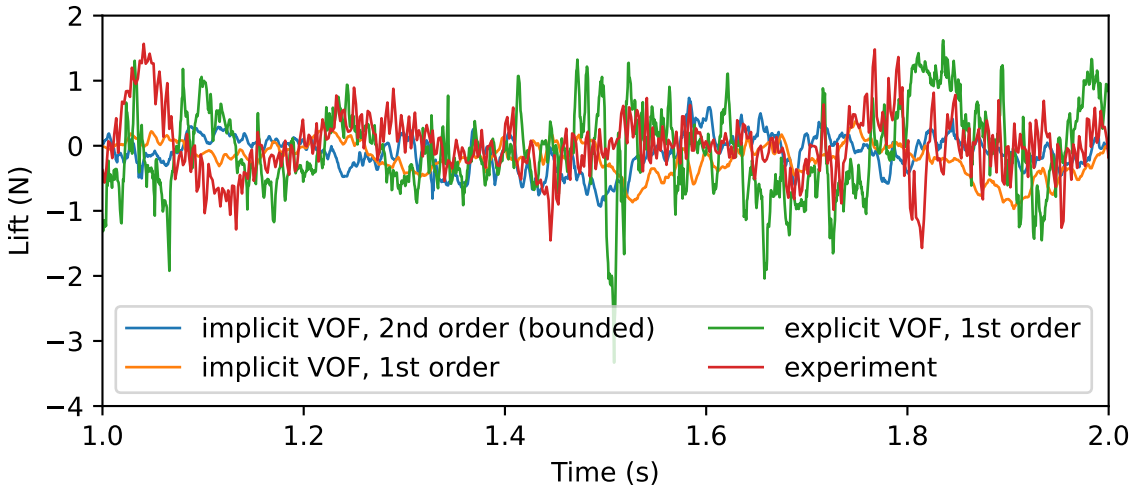

Figure 6: A part of the time history of the lift force on the red cylinder in Figure 1.

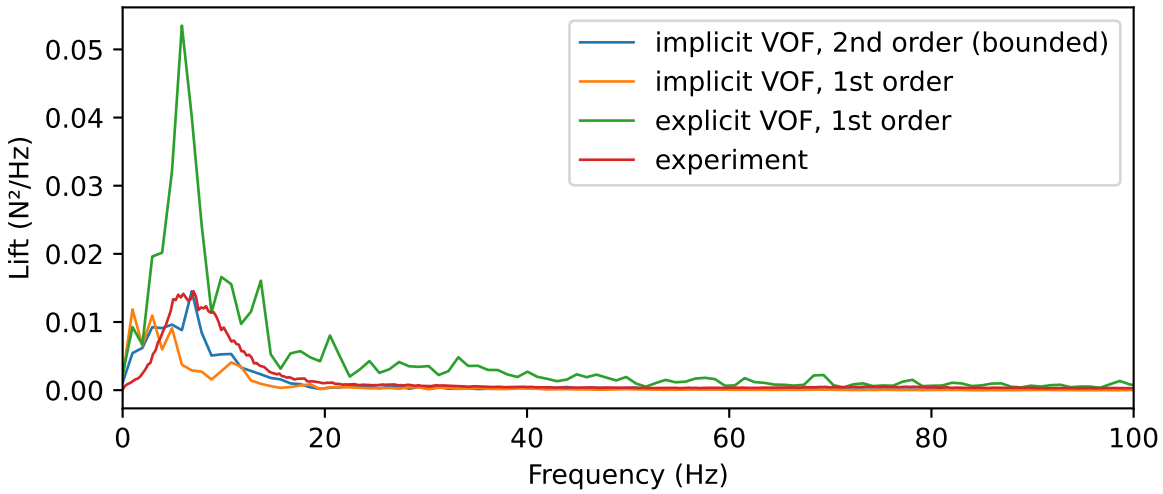

Figure 7: Power spectral density of the lift force computed using Welch's algorithm.

the explicit VOF overpredicts the amplitude. The root-mean-square (RMS) value is 0.70 N, compared to 0.45 N in the experiment. With the implicit VOF approach, a value of 0.37 N is obtained when using 2$^{\text{nd}}$ order time discretization and 0.35 N when using a 1$^{\text{st}}$ order time scheme, rather close to the experimental measurement.

4.3 Fluid-structure interaction: displacement response

For the FSI simulations only 1$^{\text{st}}$ order time discretization is used, as the 2$^{\text{nd}}$ order bounded scheme is incompatible with dynamic meshes in Fluent [12]. The simulation with the explicit VOF formulation crashed after 0.79 s. Its displacement and forces w.r.t. time are omitted in the plot not to obfuscate Figure 8, but their qualitative behavior is similar.

The displacement of the moving cylinder is plotted together with the lift force in Figure 8 for the implicit VOF formulation. The oscillation starts at about 0.2 s, upon arrival of the first bubbles. The vibration has a high frequency behavior, carried by a lower frequency signal. The fluctuating lift force is directly responsible for this low frequency evolution, as is evident from Figure 8 plotting force and displacement together, while the high frequency component is related to the natural frequency of the cylinder.

The power spectral density of the displacement (Figure 9) confirms this observation. Note that the first 400 time steps were excluded to calculate the PSD and RMS values. One can observe a low frequency plateau in the 10 Hz–20 Hz band, the same band as observed earlier in Figure 7, followed by a peak at about 20 Hz–21.5 Hz. This peak corresponds to the natural frequency (22.5 Hz), slightly lowered due to the added mass effect.

The logarithmic scale of Figure 9 somewhat obscures the difference in amplitude obtained with the implicit VOF approach versus the explicit one, especially because they display very similar trends. But with an RMS of 0.039 mm for the explicit VOF approach versus 0.023 mm for the implicit VOF approach, it becomes clear that also in a coupled simulation the explicit approach yields higher amplitude forces, resulting in higher amplitude displacements.

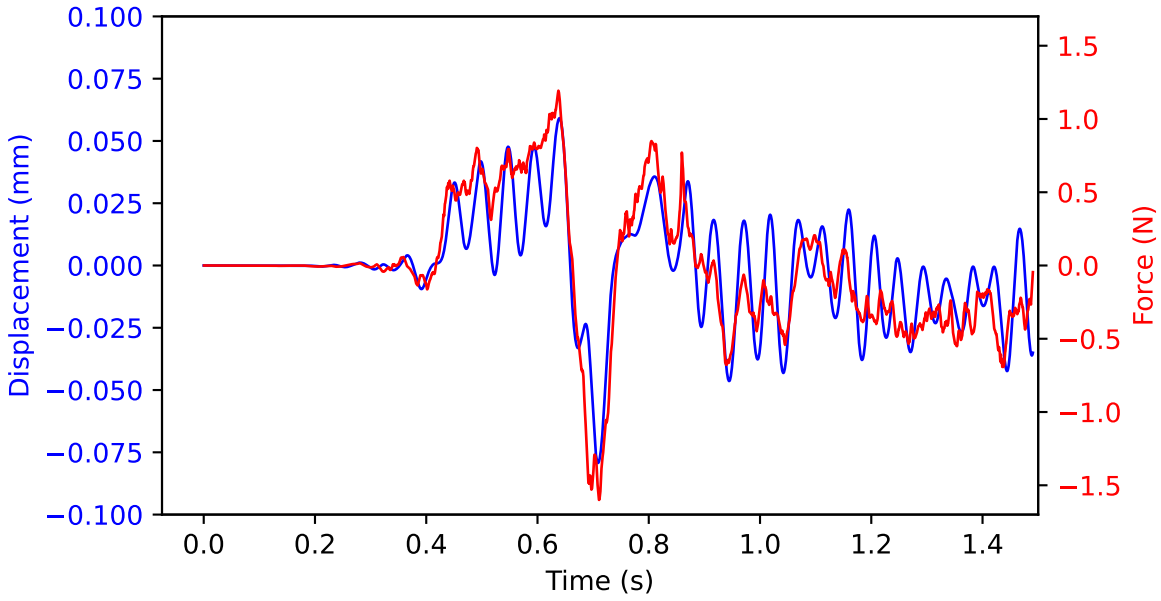

Figure 8: The displacement (blue) plotted together with the lift force (red) for the simulation using the implicit VOF formulation, 1st order in time.

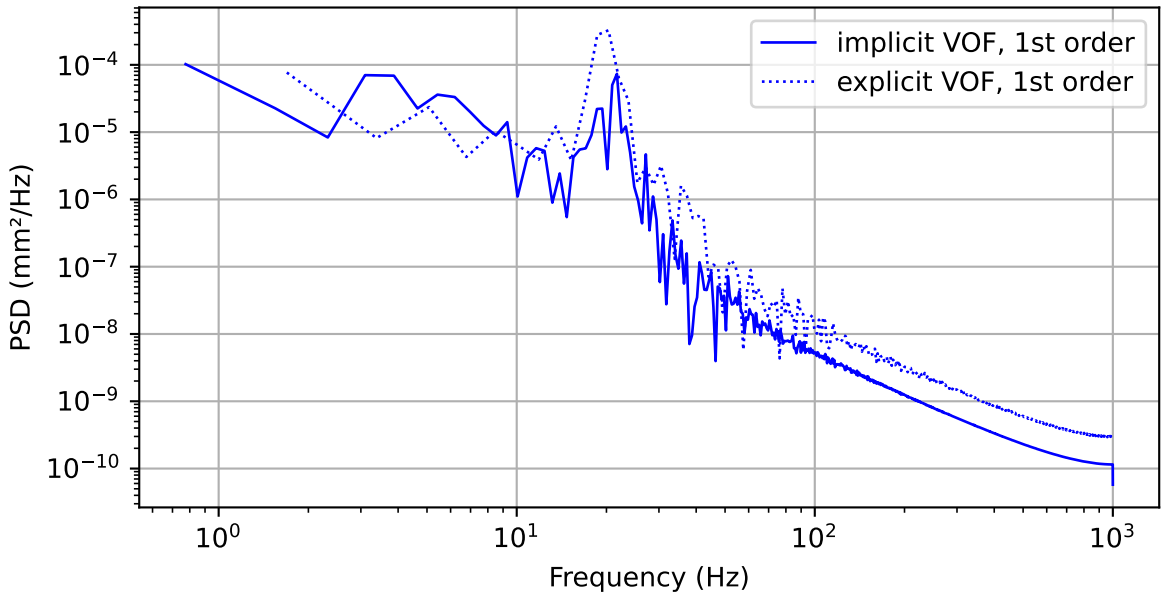

Figure 9: The power spectral density of the displacement.

4.4 Computational cost

The computational cost of a flow-only simulation of 5 s (10 000 time steps) on 384 AMD EPYC 7763 cores was about 35 h using implicit VOF and 27 h using explicit VOF. The explicit VOF does not add a system equation for the indicator function (e.g. α_{air}), resulting in a smaller system to be solved.

For the FSI simulation, 1.49 s of flow time was obtained in 72 h on 640 AMD EPYC 7763 cores.

A virtual pre-domain for 6 s (12 000 time steps) was independently generated beforehand on a single Intel Xeon Gold 6242R core in 23 min, orders of magnitude smaller than the cost of using an actual precursor domain to develop the flow.

5 CONCLUSIONS

This paper discusses the use of a modified version of the Synthetic Bubble Model of De Moerloose et al. [2] for a tube bundle in cross-flow. The SBM, originally developed for OpenFOAM, was implemented in Fluent and the generation of the virtual pre-domain was accelerated. The size of the tube bundle was significantly larger than tested before [2].

Encouraging results were obtained as the SBM was able to generate a transient inlet profile of randomly distributed bubbles, providing realistic loads on the tube bundle structure without having to rely on a computationally expensive precursor simulation domain to develop the flow. The evolution of the bubbles as they move through the domain was heavily dependent on the VOF formulation, resulting in amplitude differences in forces and displacements of about a factor of 2. However, this behavior was not related to the use of the SBM and were still reasonably close to experimental measurements.

Possible effects of the grid size and time step size were not yet investigated. Diffusion may be the result of a too coarse grid or a too large time step. A smaller time step might also stabilize the explicit VOF approach. Further study may shed light on these effects, but the computational burden of such refinements should however be balanced with the primary purpose of this research: evaluating the FIV in the bundle.

Given the scarcity of numerical simulations of two-phase flow-induced vibrations, the results obtained in this work, which represents the first use of the SBM in an FSI simulation, are promising for the use of the SBM in future research.

ACKNOWLEDGMENTS

This project (GO-VIKING) has received funding from the European Union's Horizon Europe research and innovation program under grant agreement No 101060826.

The computational resources and services used in this work were provided by the VSC (Flemish Supercomputer Center), funded by the Research Foundation Flanders (FWO), Belgium and the Flemish Government - department EWI, Belgium.

REFERENCES

[1] A. Ono, S. Yamashita, T. Suzuki and H. Yoshida, Numerical simulation of two-phase flow in 4x4 simulated bundle. *Mech. Eng. J.* , Vol. **7**(3), 2020.

[2] L. De Moerloose, A. Bral, T. Demeester, M. De Paepe and J. Degroote, Effect of a new synthetic bubble model on forces in simulations of two-phase flows in tube bundles. *Eur. J. Mech.*, Vol. **90**, pp. 49–62, 2021.

[3] L. De Moerloose, H. Dolfen, M. De Paepe and J. Degroote. Forces and displacements in a bend subjected to an air-water flow. *12th International Conference on Flow-Induced Vibration*, Paris-Saclay, France, 2022.

[4] A.A. Ala, S. Tan, S. Qiao and G.A. Shiru. Simulation of the effect of partial and total blockage of a sub-channel on two-phase flow through a 5 x 5 square rod bundle. *Prog. Nuclear Energy*, **155**, 104514, 2023.

[5] W. Benguigui, S. Benhamadouche, F. Beltran and M. Hassan. Experimental and numerical contributions on flow-induced vibration in steam-generator-like tube bundles: A review. *Nucl. Eng. Des.*, **424**, 113305. 2024.

[6] International Atomic Energy Agency. Status of Fast Reactor Research and Technology Development. 2013.

[7] A. Papukchiev, K. Zwijsen, D. Vivaldi, H. Hadžić, S. Benhamadouche, W. Benguigui and P. Planquart. The European GO-VIKING project on flow-induced vibrations: overview and current status. *Kerntechnik*, **89**(2), pp. 107-123. 2024.

[8] W. Benguigui and F. Beltran, Analysis of cylinder force spectrum dependency to flow pattern, in a rotated triangular tube bundle subjected to air-water cross-flow. *10th International Symposium on Fluid-Structure Interactions, Flow-Sound Interactions, Flow-Induced Vibration & Noise*, Iguaçu Falls, Brazil. 2024.

[9] W. Benguigui. Numerical simulation of two-phase flow induced vibration. PhD Thesis. Université Paris-Saclay. 2018.

[10] O. Sadek, A. Mohany and M. Hassan. Numerical investigation of the cross flow fluidelastic forces of two-phase flow in tube bundle. *J. Fluids Struct.*, **79**, pp. 171-186. 2018.

[11] D. Panunzio, R. Lagrange, P. Piteau, X. Delaune and J. Antunes. Experimental investigation of cross-flow fluidelastic instability for rotated triangular tube bundles subjected to single-phase and two-phase transverse flows. *12th International Conference on Flow-Induced Vibration*, Paris-Saclay, France, 2022.

[12] ANSYS. Ansys Fluent Theory Guide (2023R1). 2023.

[13] J. Vierendeels, K. Dumont, E. Dick and P. Verdonck, Analysis and Stabilization of Fluid-Structure Interaction Algorithm for Rigid-Body Motion. *AIAA Journal*, Vol. **43**(12), pp. 2549-2557, 2005.

[14] P. Piteau, X. Delaune, L. Borsoi and J. Antunes, Experimental identification of the fluidelastic coupling forces on a flexible tube within a rigid square bundle subjected to single-phase cross-flow. *J. Fluids Struct.*, Vol. **86**, pp. 156-169, 2019.